Inorganic Chemistry
Article

Inorg. Chem. **2010**, *49*, 5603–5610 **5603**
DOI: 10.1021/ic100488t

Synthesis, Characterization, and Crystallographic Study of the $PbO-Bi_2O_3-V_2O_5$ System: $Pb_{3-x}Bi_{2x/3}V_2O_8$ ($0.20 \leq x \leq 0.50$)

Prangya Parimita Sahoo,[†] Etienne Gaudin,[‡] Jacques Darriet,[‡] and T. N. Guru Row*,[†]

[†]*Solid State and Structural Chemistry Unit, Indian Institute of Science, Bangalore 560012, India, and*
[‡]*CNRS, Université de Bordeaux, ICMCB, 87 Avenue du Dr. A. Schweitzer, Pessac F-33608, France*

Received March 17, 2010

A new solid solution $Pb_{3-x}Bi_{2x/3}V_2O_8$ ($0.20 \leq x \leq 0.50$), stabilizing the high-temperature γ form of $Pb_3V_2O_8$, has been isolated in the system $Pb_3V_2O_8-BiVO_4$. The single-crystal structure of the composition $x = 0.50$ ($Pb_{2.5}Bi_{1/3}V_2O_8$) was solved using single-crystal X-ray diffraction (XRD) technique. The compound crystallizes in the trigonal crystal system $R\bar{3}m$ (No. 166) with a palmierite structural type with $a = 5.7463(3)$ Å, $c = 20.3047(12)$ Å, $V = 580.64(5)$ Å^3, and $Z = 3$. The final R1 value of 0.0406 was achieved for 217 independent reflections during the structure refinement. The variable-temperature powder XRD shows the absence of any phase transition for all of the members of the solid solution in the limit of 398−80 K. The new solid solution has been characterized by neutron powder diffraction, solid-state UV−vis diffuse-reflectance spectra, scanning electron microscopy, and X-ray photoelectron spectroscopy (XPS). Alternating-current impedance studies indicate conductivity on the order of $10^{-4}\ \Omega^{-1}\ cm^{-1}$ for $Pb_{2.5}Bi_{1/3}V_2O_8$. The change in color of the samples from brown to yellow at high temperature was explained by XPS studies, which indicate the plausible formation of the ppm level of Bi_2O_3 at such elevated temperature ranges.

Introduction

$Pb_3V_2O_8$ is a well-studied compound among lead vanadates owing to the display of interesting phase transitions with temperature. This compound undergoes two first-order phase transitions at 373 and 273 K.[1] Above 373 K, it crystallizes in a rhombohedral γ phase with the space group $R\bar{3}m$, at room temperature, it is monoclinic (β phase) $P2_1/c$, and below 273 K, it is $A2$ (α phase). The γ, β, and α phases are paraelastic−paraelectric, ferroelastic−antiferroelectric, and ferroelastic−ferroelectric, respectively. Variable-temperature single-crystal and powder X-ray diffraction (XRD) studies along with electron diffraction studies have been carried out to establish the nature of the phase transitions unequivocally.[2−7] The electronic lone pairs of the Pb atoms direct the structural evolution of $Pb_3V_2O_8$, and these phase transitions have been compared with the martensitic transformations where weak electronic interactions are involved.[3] Dielectric and dilatometric measurements have been performed to determine the pressure−temperature diagram.[8] Raman studies corroborate the ferroelectric nature of the phase transitions.[9,10]

Among the three phases, the γ phase of $Pb_3V_2O_8$ belongs to the palmierite types of compounds and is isostructural with a series of compounds with the general formula $A_3M_2O_8$ (A = Sr, Ba; M = P, V, As, Cr) and with that of the high-temperature phase of $Pb_3P_2O_8$.[11−13] Substitutions at all of the three sites have been reported in the literature. For example, structure property correlations in $Ba_2La_{2/3}V_2O_8$, $Sr_2La_{2/3}V_2O_8$ (substitution at the A site), $Pb_3(V,P)O_8$, $Ba_3(W,Nb)_2O_8$ (substitution at the M site), and $Ba_3W_2O_6N_2$ (substitution at the O site) have been described in detail.[14−19]

In the case of substitution at the A site, cation vacancies are created because of aliovalent substitution. Ionic and electronic conductivities have been observed for a range of

*To whom correspondence should be addressed. E-mail: ssctng@sscu.iisc.ernet.in. Phone: +91-80-22932796. Fax:+91-80-23601310.

(1) Isupov, V. A.; Krainik, N. N.; Fridberg, I. D.; Zelenkova, I. E. *Sov. Phys. Solid State, USSR* **1965**, *7*, 844.
(2) Garnier, P.; Calvarin, G.; Berar, J. F.; Weigel, D. *Mater. Res. Bull.* **1984**, *19*, 407.
(3) Kiat, J. M.; Garnier, P.; Pinot, M. *J. Solid State Chem.* **1991**, *91*, 339.
(4) Kasatani, H.; Umeki, T.; Terauchi, H. *J. Phys. Soc. Jpn.* **1992**, *61*, 2309.
(5) Kasatani, H.; Umeki, T.; Terauchi, H.; Ishibashi, Y. *J. Phys. Soc. Jpn.* **1991**, *60*, 1169.
(6) Manolikas, C.; Amelinckx, S. *Phys. Status Solidi A* **1980**, *60*, 607.
(7) Manolikas, C.; Amelinckx, S. *Phys. Status Solidi A* **1980**, *61*, 179.
(8) Midorikawa, M.; Kashida, H.; Sawada, A.; Ishibashi, Y. *J. Phys. Soc. Jpn.* **1980**, *49*, 1095.
(9) Kuok, M. H.; Lee, S. C.; Tang, S. H.; Midorikawa, M.; Ishibashi, Y. *Solid State Commun.* **1988**, *66*, 1035.
(10) Kuok, M. H.; Lee, S. C.; Tang, S. H.; Ishibashi, Y. *Solid State Commun.* **1989**, *71*, 797.
(11) Durif, A. *Acta Crystallogr.* **1959**, *12*, 420.
(12) Susse, P.; Buerger, M. J. *Z. Kristallogr.* **1970**, *131*, 161.
(13) Brixner, L. H.; Biersted, P.; Jaep, W. F.; Barkley, J. R. *Mater. Res. Bull.* **1973**, *8*, 497.
(14) Antonov, V. A.; Arsenev, P. A.; Tadzhiaglaev, K. G. *Zh. Neorg. Khim.* **1986**, *31*, 2440.
(15) Skakle, J. M. S.; Coats, A. M.; Marr, J. *J. Mater. Sci.* **2000**, *35*, 3251.
(16) Hodenberg, R. V.; Salje, E. *Mater. Res. Bull.* **1977**, *12*, 1029.
(17) Salje, E.; Hodenberg, R. V. *J. Appl. Crystallogr.* **1977**, *10*, 132.
(18) Kemmlersack, S.; Treiber, U. *Z. Anorg. Allg. Chem.* **1981**, *478*, 198.
(19) Herle, P. S.; Hegde, M. S.; Subbanna, G. N. *J. Mater. Chem.* **1997**, *7*, 2121.

Published on Web 05/27/2010

temperatures and pressures for solid solutions like $A_{3-3x}La_{2x}V_2O_8$ (A = Ba, Sr, Ca).[20−22] Recently, a series of compounds with the formula $Sr_{3-3x}La_{2x}(V_{1-y}P_yO_4)_2$ have been synthesized, and their electrical conductivities have been measured.[23] $Ba_3(VO_4)_2$ and Nd^{3+}-doped $Ba_3(VO_4)_2$ crystals were grown by the Czochralski method for applications in laser properties, Raman spectra characteristics, high-pressure energy-dispersive XRD measurements, and luminescent properties.[24]

A continuous solid solution exists in the case of $Pb_3V_2O_8$−$Pb_3P_2O_8$. The single crystals of different compositions of the solid solution $Pb_{3-x}P_{2x}V_{2(1-x)}O_8$ show ferroelastic phase transitions just below room temperature.[16] Elastooptic coefficients have also been determined for these single crystals.[25] A detailed structural study of this continuous solid solution has been discussed by Kiat et al.[26] All of the members of this solid solution belong to the palmierite structural type. The composition $x = 0.15$ of this solid solution exhibits phase transitions identical with those of the parent compounds, whereas for compositions $x = 0.35$ and 0.50, the structures belong to the palmierite structural type with no phase transitions at low temperature. For composition $x = 0.75$, at 85 K the structure is monoclinic, space group $C2/c$, similar to the room temperature structure of $Pb_3P_2O_8$.

The ternary system PbO−Bi_2O_3−V_2O_5 is one of the most investigated systems because it combines both Pb^{2+} and Bi^{3+} cations with active "$6s^2$" lone pairs. The stereochemical space requirement leads to structural distortions, which might result in structural phase transitions and interesting properties. Recently, polymorphism in the $PbBiVO_5$ system has been studied in detail with combined XRD and neutron powder diffraction (NPD).[27,28] A new incommensurately modulated polymorph of Pb_2BiVO_6 was isolated, and its crystal structure was determined by single-crystal XRD.[29] The conductivity properties of the new compounds $(PbBi)_{46}V_8O_y$ and $PbBi_6V_2O_{15}$ have enriched further the ternary system involving Pb and Bi cations.[30,31]

In the present study, a new solid solution, $Pb_{3-x}Bi_{2x/3}V_2O_8$ ($0.20 \le x \le 0.50$), has been isolated in the phase diagram of $Pb_3V_2O_8$−$BiVO_4$. The single-crystal structure determination revealed the subtle differences of this solid solution from the high-temperature γ form of $Pb_3V_2O_8$. However, unlike some members of the solid solution $Pb_{3-x}P_{2x}V_{2\,(1-x)}\,O_8$, the various members of this solid solution do not undergo any phase transition. We have described the single-crystal structure determination, variable-temperature powder XRD, NPD, solid-state UV−visible diffuse-reflectance spectra, X-ray photoelectron spectroscopy (XPS), scanning electron microscopy (SEM), and conductivity of the isolated new solid solution.

Experimental Section

Materials. Bi_2O_3 (Aldrich, 99.9%) was dried at 350 °C for 6 h before use. V_2O_5 (S. D. Fine-Chem Ltd., Boisar, India, 99%) and PbO (Aldrich, 99.9%) were used as received.

Preparation and Crystal Growth. Polycrystalline samples of phases $x = 0.20$, 0.25, 0.30, 0.35, 0.40, and 0.50 in the solid solution $Pb_{3-x}Bi_{2x/3}V_2O_8$ were synthesized by the solid-state route using the starting materials PbO, Bi_2O_3, and V_2O_5 in the stoichiometric ratios. The compositions of the starting reactants were initially ground well in an agate mortar and pestle. The resultant mixture was exposed to heat treatment for 2 days at 650 °C and at 700 °C for 4 h with two intermediate regrindings. All of the syntheses were carried out under an oxygen atmosphere. The color of the products obtained was brown. The progress of the reaction was monitored by powder XRD, which confirmed the formation of a single phase for the various compositions. Single crystals of the compound $Pb_{2.5}Bi_{1/3}V_2O_8$ ($x = 0.50$) were obtained by melting a polycrystalline sample at 900 °C for 2 h in a platinum crucible, followed by slow cooling at 5 °C h^{-1} up to 800 °C and then furnace cooling to room temperature.

Powder XRD. Powder XRD data were collected using a Philips X-pert diffractometer with Cu Kα radiation over the angular range $10° \le 2\theta \le 80°$, with a step width of 0.0167° at room temperature calibrated against Silicon Powder (NIST-SRM 640c) standards. Le Bail profile analysis in the *JANA2000* suite of programs was used to refine the XRD data.[32] The background was estimated by a Legendre polynomial function consisting of 15 coefficients, and the peak shapes were described by a pseudo-Voigt function, varying five profile coefficients. A scale factor, a zero error factor, and shape were refined.

Variable-temperature powder XRD data were collected at the synchrotron source at Trieste, Italy. The wavelength used for the experiment was 1.0 Å, calibrated against LaB_6 (NIST-SRM 660a) standards. The samples were loaded in a capillary after sonication. The capillary was rotated during data accumulation. The program *Fit2d* was used to integrate the data obtained from the synchrotron source.

Single-Crystal XRD. An approximately rhombohedral single crystal was selected on the basis of the size and sharpness of the diffraction spots. Data collection was carried out on an Oxford Xcalibur MOVA diffractometer with a four-circle κ goniometer employing a graphite-monochromatized Mo Kα ($\lambda_{\text{Mo K}\alpha}$ = 0.710 73 Å) radiation at 293(2) K. The diffraction intensities were corrected for Lorentz and polarization effects. The data were reduced using CrysAlis RED (special programs available with the diffractometer), the shape was determined with the video microscope attached to the diffractometer, and an analytical absorption correction (after Clark and Reid) was applied. The structure was solved by direct methods using *SHELXS97* and refined using *SHELXL97* from 217 independent reflections, having $I \ge 2\sigma(I)$.[33] The packing diagrams were generated by *DIAMOND*, version 2.1c.[34] Crystallographic data and the details of the single-crystal data collection are given in Table 1. Atomic coordinates and isotropic displacement parameters are presented in Table 2. Anisotropic displacement parameters (ADPs) and selected interatomic distances are given in Tables 3 and 4.

NPD. NPD experiments were performed on the BT-1 32 detector neutron powder diffractometer at the NCNR (NIST Centre for Neutron Research), NBSR (Neutron Beam Split-core Reactor),

(20) Leonidov, I. A.; Leonidova, O. N.; Fotiev, A. A. *Sov. Electrochem.* **1992**, *28*, 1241.
(21) Leonidov, I. A.; Leonidova, O. N.; Surat, L. L.; Samigullina, R. F. *Inorg. Mater.* **2003**, *39*, 616.
(22) Leonidov, I. A.; Leonidova, O. N.; Slepukhin, V. K. *Inorg. Mater.* **2000**, *36*, 72.
(23) Leonidova, O. N.; Leonidova, E. I. *Solid State Ionics* **2008**, *179*, 188.
(24) Gao, Z.; Guo, F.; Zhao, B.; Zhuang, N.; Chen, Y.; Liu, J.; Chen, J. *J. Cryst. Growth* **2008**, *310*, 2503.
(25) Salje, E. *Phys. Status Solidi A* **1976**, *33*, K165.
(26) Kiat, J. M.; Garnier, P.; Calvarin, G.; Pinot, M. *J. Solid State Chem.* **1993**, *103*, 490.
(27) Labidi, O.; Roussel, P.; Drache, M.; Vannier, R. N.; Wignacourt, J. P. *J. Solid State Chem.* **2008**, *181*, 2268.
(28) Labidi, O.; Roussel, P.; Porcher, F.; Drache, M.; Vannier, R. N.; Wignacourt, J. P. *J. Solid State Chem.* **2008**, *181*, 2260.
(29) Roussel, P.; Labidi, O.; Huve, M.; Drache, M.; Wignacourt, J. P.; Petricek, V. *Acta Crystallogr., Sect. B* **2009**, *65*, 416.
(30) Labidi, O.; Drache, M.; Roussel, P.; Wignacourt, J. P. *Solid State Sci.* **2008**, *10*, 1074.
(31) Labidi, O.; Drache, M.; Roussel, P.; Wignacourt, J. P. *Solid State Sci.* **2007**, *9*, 964.
(32) Dusek, M.; Petricek, V.; Wunschel, M.; Dinnebier, R. E.; van Smaalen, S. *J. Appl. Crystallogr.* **2001**, *34*, 398.
(33) Sheldrick, G. M. *Acta Crystallogr., Sect. A* **2008**, *64*, 112.
(34) Brandenburg, K. *DIAMOND*, version 2.1c; Crystal Impact GbR: Bonn, Germany, **1999**.

Gaithersburg, MD. A Ge(311) monochromator with a 75° takeoff angle, $\lambda = 2.0787(2)$ Å, and in-pile collimation of 15 min of arc were used. Data were collected over the range of $2\theta = 3.00-120°$ with a step size of 0.05°. The sample was loaded in a vanadium can sample holder of length 50 mm and diameter 6.0 mm. Data were collected under ambient conditions. The NPD data were analyzed by Le Bail profile analysis and then refined by the Rietveld method, as implemented in the *JANA2000* program suite.[32] The background was estimated by a Legendre polynomial function consisting of 15 coefficients, and the peak shapes were described by a Gaussian function, varying three profile coefficients.

Characterization. Analysis of the morphology was performed with the help of a FEI Sirion scanning electron microscope. UV−visible diffuse-reflectance spectra were recorded on a Perkin-Elmer Lambda 35 UV−visible spectrophotometer. XPS spectra were collected on a Thermoscientific Multilab 2000 equipment employing Al Kα X-rays. Binding energies reported in this paper are with reference to C 1s at 284.5 eV, and they are accurate within ±0.1 eV.

Ionic Conductivity from Alternating-Current (ac) Impedance. A circular pellet of $Pb_{2.5}Bi_{1/3}V_2O_8$ of approximately 10 mm diameter and 1 mm thickness was annealed at 800 °C for 0.5 h. Then the silver paste was applied on both sides of the pellet for ac impedance measurements. The coated pellet was heated at 150 °C for 1 h to remove the organic component of the silver paste. The annealed pellets were then placed between two steel electrodes of a home-made conductivity cell (cell constant 0.122). The temperature of the pellet was maintained at each temperature using a programmable Thermolyne furnace (error in measurement ±1 °C). The pellet was equilibrated for 0.5 h at every temperature point prior to the measurements. The ac impedance measurements were carried out on a Novocontrol Alpha-A equipment in the frequency range of $1 \times 10^0-3 \times 10^6$ Hz (signal amplitude = 0.05 V) from 30 to 500 °C at an interval of 50 °C.

Table 1. Principal Characteristics of $Pb_{2.5}Bi_{1/3}V_2O_8$ Single-Crystal XRD and NPD Structure Determination

chemical formula	$Pb_{2.5}Bi_{1/3}V_2O_8$	$Pb_{2.5}Bi_{1/3}V_2O_8$
radiation type	X-ray	neutron
fw	817.5	817.5
cryst habit, color	rhombohedral, yellow	
cryst size/mm	0.021 × 0.004 × 0.002	
temperature/K	293(2)	293(2)
wavelength/Å	0.710 73 (Mo Kα)	2.0787
monochromator	graphite	Ge(311)
cryst syst	trigonal	trigonal
space group	$R\bar{3}m$	$R\bar{3}m$
a/Å	5.7463(3)	5.76048(1)
c/Å	20.3047(12)	20.3029(1)
volume/Å^3	580.64(5)	583.453(3)
Z	3	3
density/g cm^{-3}	7.019	6.9771
$F(000)$	1028	
scan mode	ω scan	
θ_{max}/deg	29.1457	
$h_{min,max}$, $k_{min,max}$, $l_{min,max}$	(−7, 7), (−7, 7), (−26, 26)	
no. of reflns measd	2450	
no. of unique reflns	217	
abs corrn	analytical from crystal shape	
μ/mm^{-1}	64.133	
no. of param	22	31
refinement	F^2	
R_all, R_obs	0.0502, 0.0406	0.0722, 0.0632
wR2_all, wR$_2$_obs	0.1113, 0.1086	0.0609, 0.0605
GOF	1.125	2.03
max, min $\Delta\rho$/e Å^{-3}	1.941, −1.665	
R_p, wR_p		0.0559, 0.0712

Results and Discussion

Crystal Structure. Single-crystal XRD data on the composition $x = 0.50$ of the solid solution $Pb_{2.5}Bi_{1/3}V_2O_8$ were indexed into the trigonal crystal system, with $a = 5.7463(3)$ Å, $c = 20.3047(12)$ Å, $V = 580.64(5)$ Å^3, and $Z = 3$. Space group $R\bar{3}m$ was assigned based on the systematic absences. The positions of the heavy atoms were obtained by direct methods. Four different models of refinement were carried out in order to obtain the most suitable crystallographic parameters. No reflections were omitted in any of the refinement protocols. The high-temperature γ form of $Pb_3V_2O_8$ was taken as model 1. In this model, Bi was not incorporated. Pb(1) was located at the 3a site, whereas the Pb(2) and V atoms occupied two different 6c sites. Subsequent difference Fourier synthesis revealed the remaining O atoms. While one O atom occupies the 6c site, the other one occupies the 18h site. The structure was refined with the formula $Pb_3V_2O_8$ with full occupancies assigned to all of the atoms. At this stage of refinement, the reliability factor ($R_1 = 0.1170$) and residual electron density ($\Delta\rho = 7.24, -6.59$ e Å^{-3}) were very high. In model 2, Pb(2) was located in site 18h and not in site 6c with an occupancy of $^1/_3$. This enormously reduced the reliability factor ($R_1 = 0.0455$) and residual electron density ($\Delta\rho = 1.60, -2.02$ e Å^{-3}). In order to account for the Bi present in the crystal, two more refinement models were tried with Bi in the Pb(1) and Pb(2) positions. In model 3, Bi shares the same site as that of Pb(1), with the occupancies of Pb(1) and Bi(1) being 0.5 and $^1/_3$ and the remaining

Table 2. Atomic Coordinates (Å) and Isotropic Displacement Parameters (Å^2) for $Pb_{2.5}Bi_{1/3}V_2O_8$ Obtained from Single-Crystal XRD

atomic and Wyckoff positions	x	y	z	U_{eq} (Å^2)	occupancy
Pb(1) (3a)	0	0	0	0.0613(5)	1
Pb(2) (18h)	0.70125(14)	−0.70125(14)	0.12953(6)	0.0433(7)	0.25
Bi(2) (18h)	0.70125(14)	−0.70125(14)	0.12953(6)	0.0433(7)	0.0555
V(1) (6c)	$^1/_3$	$-^1/_3$	0.06930(12)	0.0201(6)	1
O(1) (6c)	$^1/_3$	$-^1/_3$	−0.0115(7)	0.066(4)	1
O(2) (18h)	0.1718(8)	−0.1718(8)	0.0974(4)	0.047(3)	1

Table 3. ADPs (Å^2) of $Pb_{2.5}Bi_{1/3}V_2O_8$ Obtained from Single-Crystal XRD

atomic and Wyckoff positions	U_{11}	U_{22}	U_{33}	U_{23}	U_{13}	U_{12}
Pb(1) (3a)	0.0603(8)	0.0603(8)	0.0635(10)	0	0	0.0302(4)
Pb(2) (18h)	0.0444(16)	0.0444(16)	0.0351(7)	0.0040(6)	−0.0040(6)	0.0177(5)
Bi(2) (18h)	0.0444(16)	0.0444(16)	0.0351(7)	0.0040(6)	−0.0040(6)	0.0177(5)
V(1) (6c)	0.0201(8)	0.0201(8)	0.0202(13)	0	0	0.0101(4)
O(1) (6c)	0.087(8)	0.087(8)	0.025(7)	0	0	0.044(4)
O(2) (18h)	0.053(4)	0.053(4)	0.052(5)	−0.0035(19)	0.003(4)	0.0383(19)

Table 4. Selected Bond Lengths of $Pb_{2.5}Bi_{1/3}V_2O_8$

bond length type	distance (Å)
V(1)−O(1)	1.641(15)
V(1)−O(2) (×3)	1.706(8)
Pb(1)−O(2) (×6)	2.614(8)
Pb(2)/Bi(2)−O(1) (×1)	2.420(14)
Pb(2)/Bi(2)−O(2) (×3)	2.668(8)
Pb(2)/Bi(2)−O(2) (×6)	2.961(8)

parameters the same as those of model 2. This refinement increased the residual factor ($R_1 = 0.0855$) and residual electron density ($\Delta\rho = 7.46, -2.41$ in e Å^{-3}). In model 4, Bi and Pb(2) were assigned to the same 18h site. The occupancies of Pb(2) and Bi(2) were 0.25 and 0.056, respectively. The residual factor and residual electron density were $R_1 = 0.0406$ and $\Delta\rho = 1.941, -1.665$ e Å^{-3}, respectively. Model 4 was taken as the final refinement model. The difference Fourier maps of models 1 and 4 are presented in Figure 1. The electron density has been properly modeled in the case of model 4, as is evident from the figure. From all of these refinement models, it can be concluded that the Pb(2) position is split and Bi is located on this site and not on the Pb(1) site. In $Pb_3V_2O_8$ during the transition from the γ to β phase, the coordination environment surrounding Pb(2) undergoes a large distortion compared to the Pb(1) and V atoms.[3] This might explain the preference of the Bi atom to the Pb(2) position rather than the Pb(1) position. For example, in compound $Ba_2Nd_{2/3}V_2O_8$, the Nd^{3+} cation shares the Ba(2) position and not the Ba(1) position.[15] In the present study, it may be noted that the coordination environment around the Pb(2) atom is 10-fold with three kinds of bond distances, suggesting that this position is more likely to accommodate the Bi atom than the more stable octahedral Pb(1) position. This explains the difference in the *R* factors between our models 2 and 3. Substitution of Bi^{3+} to Pb^{2+} leads to a decrease of the occupancy ratio of the Pb position in $Pb_3V_2O_8$. In model 3, the overall occupancy of the Pb1/Bi1 position is equal to 83.3%, with a full occupancy for Pb2. In model 4, the overall occupancy of Pb2/Bi2 is equal to 91.7%, with a full occupancy for Pb1. Between models 2 and 4, there is not much difference between the *R* factors (0.0455 for model 2 and 0.0406 for model 4). However, because incorporation of Bi^{3+} stabilizes the high-temperature form, we have tried to incorporate Bi^{3+} in the structure refinement to account for the Bi incorporation as per the formula.

The general view of the palmierite structure along the *c* direction is described in Figure 2. The structure consists of $[VO_4]^{3-}$ tetrahedra. The coordination around the two kinds of Pb and Pb/Bi atoms is different. The Pb(1) atom occupying the $\bar{3}$m position forms an octahedron with the O(2) atoms. In the palmierite γ-$Pb_3V_2O_8$ structure, the Pb(2) atom occupies the 3m position, but in the present case, because of incorporation of Bi, the symmetry was lowered only to a mirror symmetry. Pb(2)/Bi(2) has 10-coordination of the O atoms surrounding it. Figure 3 depicts the coordination environment surrounding each atom in the crystal lattice. $[VO_4]^{3-}$ tetrahedra have their vertices in the opposite directions, as seen from Figure 3. The similarity between the 9R polytype of the hexagonal perovskite and the palmierite structure can be realized in Figure 4. In the 9R structure of $BaRuO_3$, the $(hhc)_3$

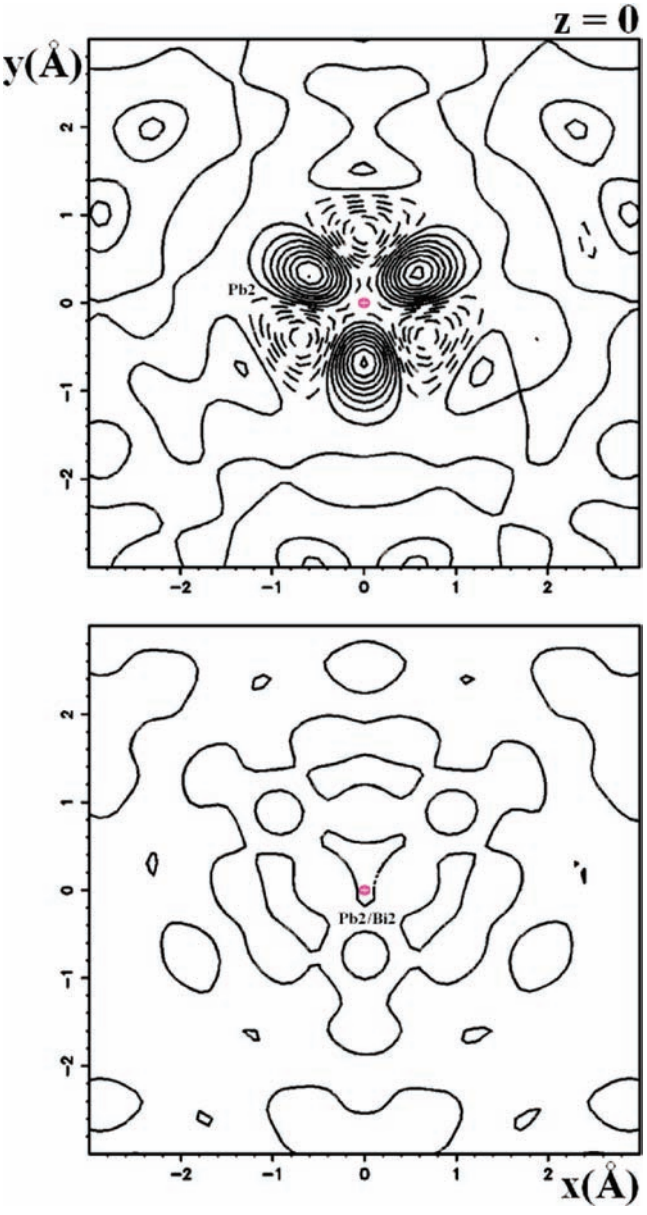

Figure 1. *xy* section of the difference Fourier maps (Å) around Pb(2) (top) for model 1 and Pb(2)/Bi(2) (bottom) for model 4 with $z = 0$. Contour lines in the interval of 1 e Å^{-3}.

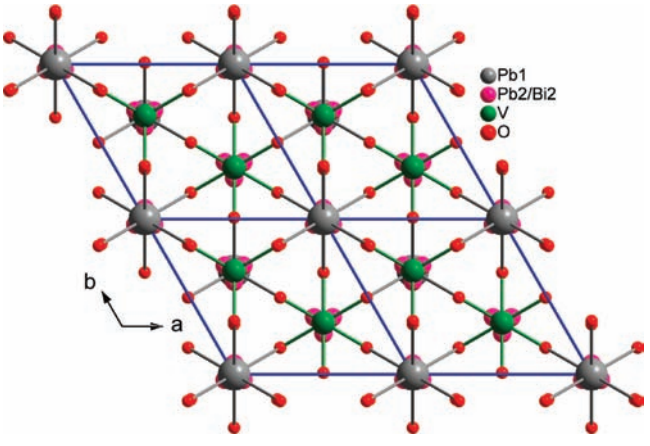

Figure 2. Two-dimensional view of the compound $Pb_{2.5}Bi_{1/3}V_2O_8$.

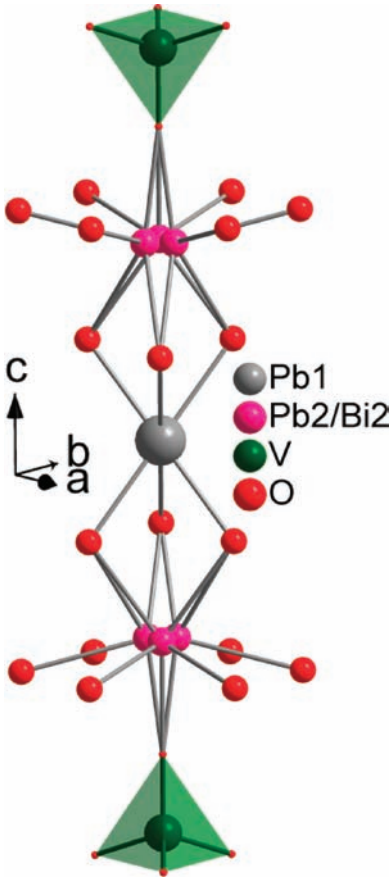

Figure 3. Coordination environment around the two crystallographically different Pb(1) and Pb(2)/Bi(2) sites.

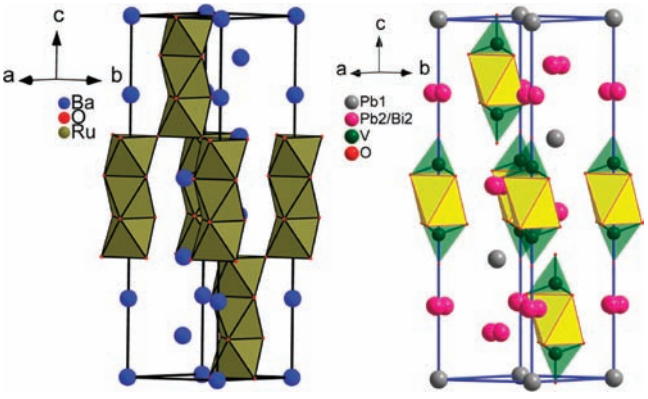

Figure 4. Structure of the 9R polytype $BaRuO_3$ with RuO_3 octahedra drawn in khaki (left). Structure of the palmierite $Pb_{2.5}Bi_{1/3}V_2O_8$ with VO_4 tetrahedra drawn in green and empty octahedra drawn in yellow (right). In both pictures, the spheres correspond to Ba(1), Ba(2), Pb(1), or Pb(2)/Bi(2) positions.

stacking of BaO_3 layers manages an octahedral site for Ru.[35] In the palmierite structure of $Pb_{2.5}Bi_{1/3}V_2O_8$, the same stacking of layers with composition PbO_2 and $(Pb/Bi)O_3$ manages a tetrahedral site filled by a V atom and an empty octahedral site.

There are two kinds of V−O distances in $[VO_4]^{3-}$ tetrahedra, making the tetrahedra distorted. The distance V−O(1) [the O atom shared by both Pb(2)/Bi(2) and V] is shorter compared to the rest of the three bond distances,

(35) Darriet, J.; Subramanian, M. A. *J. Mater. Chem.* **1995**, *5*, 543.

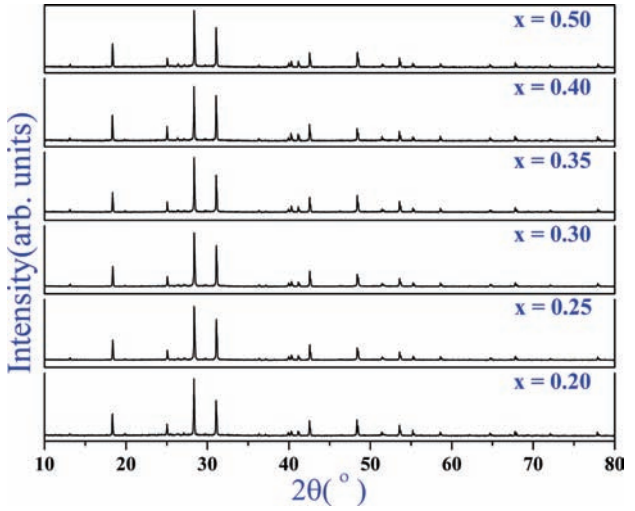

Figure 5. Powder XRD profiles of various members of the solid solution $Pb_{3-x}Bi_{2/3x}V_2O_8$ ($0.20 \le x \le 0.50$).

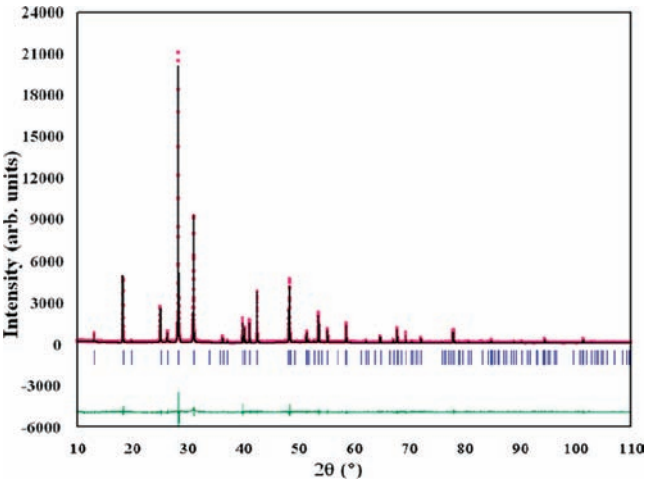

Figure 6. Profile refinement on the XRD data for the composition $x = 0.50$.

which are equal to 1.641(15) and 1.706(8) Å, respectively. The Pb(1) site forms a perfect octahedron with six equal bond distances of 2.614(8) Å. However, for the Pb(2)/Bi(2) site, there are three unique sets of bond distances. As in the case of the V−O(1) distance, Pb(2)/Bi(2)−O(1) is the shortest of all three distances, with a bond length of 2.420(14) Å. There are two kinds of Pb(2)/Bi(2)−O(2) distances. Three bond lengths equal 2.668(8) Å, and six bond distances equal 2.961(8) Å. Among them, the latter form a hexagon surrounding Pb(2)/Bi(2). All of these bond distances contribute to the 10-coordination surrounding Pb(2)/Bi(2).

Laboratory and Variable-Temperature Synchrotron XRD Data. Laboratory powder XRD confirmed the phase purity of the various compositions in the series $Pb_{3-x}Bi_{2x/3}V_2O_8$ ($0.20 \le x \le 0.50$). Figure 5 shows the powder XRD profiles of various members of the solid solution $Pb_{3-x}Bi_{2/3x}V_2O_8$ ($0.20 \le x \le 0.50$). For the composition $x = 0.50$ profile-refinements on powder XRD data were carried out using *JANA2000*, using the structural model obtained from the single-crystal data of the same composition. The observed, calculated, and difference profiles are presented in Figure 6. The changes in the cell parameters for all of the compositions were obtained following profile refinements for each

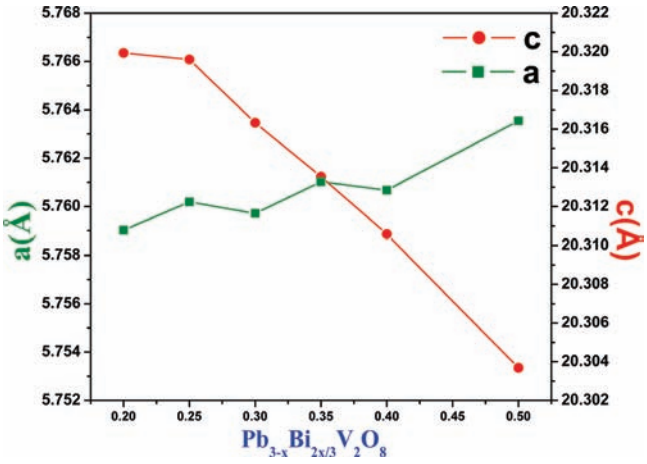

Figure 7. Variations in the cell parameters with the composition.

composition. Figure 7 describes the changes in the cell parameters in the *a* and *c* axes. While the length of the *a* axis increases, the length of the *c* axis decreases with the composition, indicating an opposite trend in the *a* and *c* axes with an increase in the Bi content in the series $Pb_{3-x}Bi_{2x/3}V_2O_8$ ($0.20 \le x \le 0.50$). However, the percentage changes in the *a* and *c* axes are nearly the same.

To establish the nature of the compositions below and above the limits of the solid solution, we have synthesized various compositions below $x = 0.20$ and above $x = 0.50$. Compositions below the value of $x = 0.20$ present a mixture of two phases, with one phase being the palmierite phase and the other one being the room temperature monoclinic β-$Pb_3V_2O_8$. Figure S1 in the Supporting Information presents the profile fitting for the composition $x = 0.10$, where the powder pattern is a mixture of two phases. The compositions above the value of $x = 0.50$ also have two phases, with one being the palmierite phase and the other being the eulytite $Pb_3BiV_3O_{12}$ phase. A detailed structural report for the phase $Pb_3BiV_3O_{12}$ has been published elsewhere.[36] Figure S2 in the Supporting Information describes the presence of two phases for the composition $x = 0.75$ in the series $Pb_{3-x}Bi_{2x/3}V_2O_8$.

Variable-temperature synchrotron powder XRD data from 398 to 80 K were collected for the highest and lowest limits of the solid solution. For both compositions $x = 0.20$ and 0.50, no phase transitions were observed down to 80 K. This experiment proves stabilization of the high-temperature γ form of $Pb_3V_2O_8$ with incorporation of Bi in the Pb site for $Pb_{3-x}Bi_{2x/3}V_2O_8$ ($0.20 \le x \le 0.50$). Figure 8 indicates the absence of phase transitions in compositions $x = 0.20$ and 0.50, respectively.

NPD Data. NPD data for the composition $x = 0.50$ ($Pb_{2.5}Bi_{1/3}V_2O_8$) at ambient conditions were collected. Rietveld refinements were carried out using *JANA2000*, using the structural model obtained from the single-crystal data of the same composition. The coordinates and thermal parameters of the V atom were fixed at the values obtained from the X-ray refinement results, because the V atom is invisible to neutron radiation. Attempts to refine Pb(2) and Bi(2) independently resulted in nonpositive definite values of the thermal parameters of Bi(2). So, the coordinates of Bi(2) and

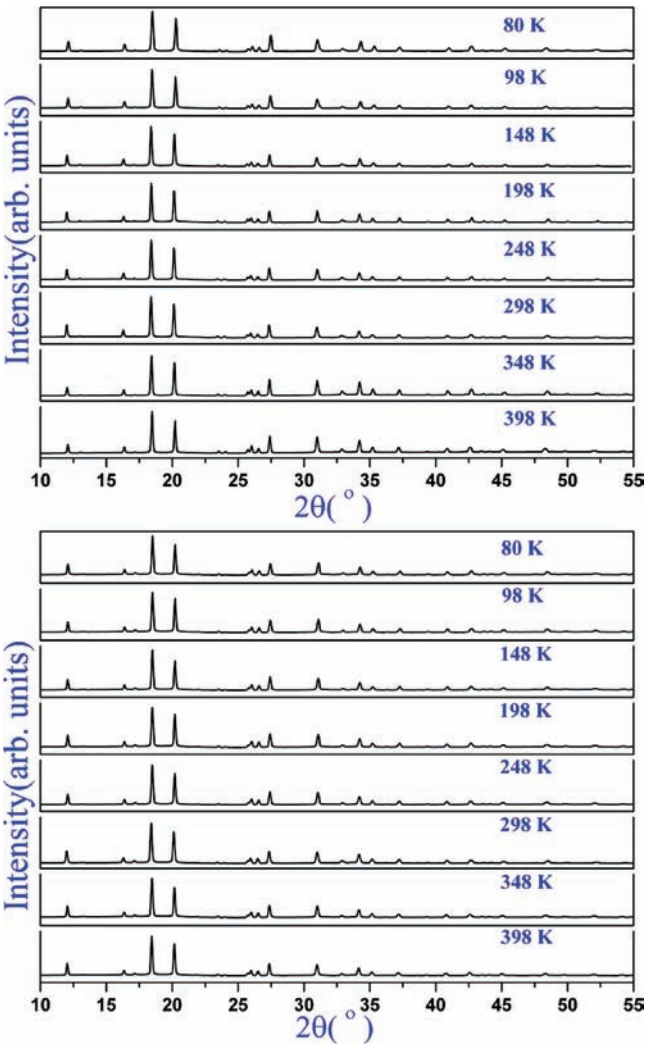

Figure 8. Temperature evolution of the composition $x = 0.20$ (above) and 0.50 (below) in the series $Pb_{3-x}Bi_{2/3x}V_2O_8$.

Pb(2) were assigned the same values. Because of the strong correlation between Pb(2) and Bi(2) in the system and about a 10% difference in the neutron scattering length of Pb and Bi ($b_{Pb} = 9.40 \times 10^{-15}$ m; $b_{Bi} = 8.85 \times 10^{-15}$ m), it is difficult to avoid constraints between Bi(2) and Pb(2) during the neutron powder refinement cycles. The crystallographic details and experimental parameters are given in Table 1. The observed, calculated, and difference profiles are presented in Figure 9.

UV−Visible Spectra, XPS, and Morphology. Room temperature UV−visible spectra were collected in the diffuse-reflectance mode for various compositions in the series $Pb_{3-x}Bi_{2/3x}V_2O_8$. The diffuse-reflectance spectra were converted to absorbance-like spectra using the Kubelka−Munk function (Figure 10). All of the spectra show a broad absorption band starting from 800 to 200 nm. The experimental band gaps for these compositions were calculated to be 3.1−3.3 eV. Figure S3 in the Supporting Information describes the SEM image for a single crystal for the composition $x = 0.50$.

During the synthesis of the different compositions, it was observed that if the compositions were heated above 800 °C, the color changed from brown to yellow without any change in the powder XRD pattern. To investigate

(36) Sahoo, P. P.; Gaudin, E.; Darriet, J.; Row, T. N. G. *Mater. Res. Bull.* **2009**, *44*, 812.

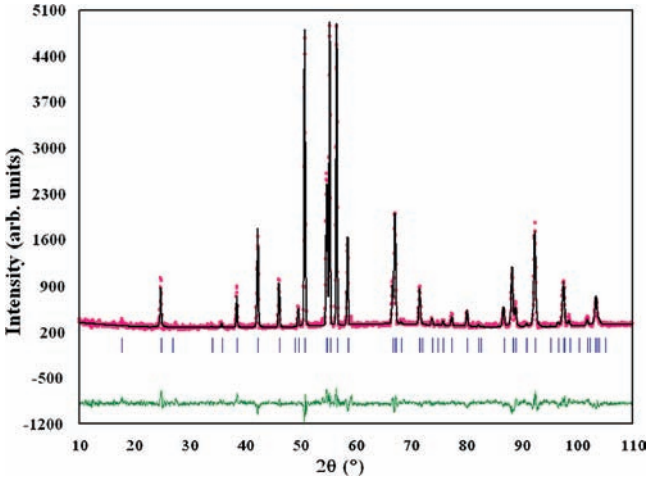

Figure 9. Observed, calculated, and difference NPD patterns for $Pb_{3-x}Bi_{2/3x}V_2O_8$ for $x = 0.50$.

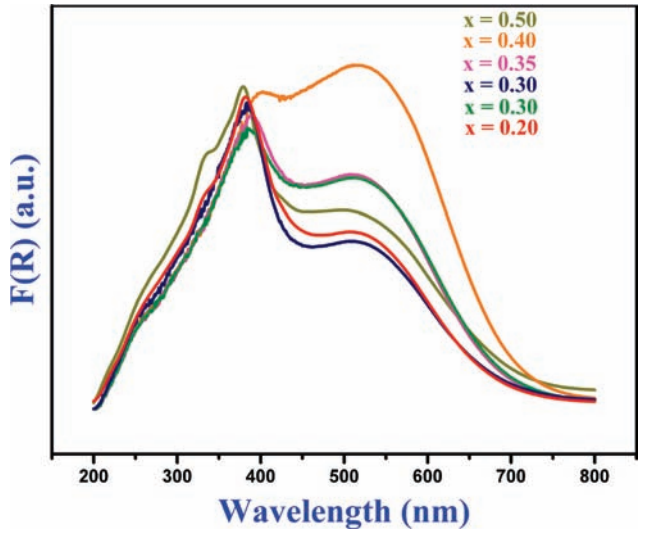

Figure 10. UV−visible diffuse-reflectance spectra for various members of the solid solution.

the possible explanation for the color change, we performed XPS analysis for the composition $x = 0.50$ before and after sintering at 800 °C for a few hours. Pb $4f_{5/2}$ and $4f_{7/2}$ binding energies are 143 and 138 eV, respectively, whereas Bi $4f_{5/2}$ and $4f_{7/2}$ binding energies are 164 and 159 eV, respectively. Core-level XPS spectra of Pb and Bi 4f before and after sintering of the sample are presented Figure 11. The intensity ratio of Pb and Bi 4f before sintering at 800 °C and after sintering is different. The 4f level of intensity of Bi was much higher in the sintered sample than in the one that was not sintered. This indicates that the ppm level of Bi is discharged from the compound forming bismuth oxide, which is below the recognition limits of powder XRD. Because the XPS technique is surface-sensitive, it is possible to detect the ppm level of bismuth oxide, which is released when the various members of this solid solution are sintered. Because bismuth oxide is yellow in color, it is assumed that the color change at higher temperature is due to the presence of the ppm level of bismuth oxide on the surface. In the literature, it is well-known that, because of the presence of a foreign atom, less than 1% in a compound is sufficient to colorize the compound. For example, the crystals of

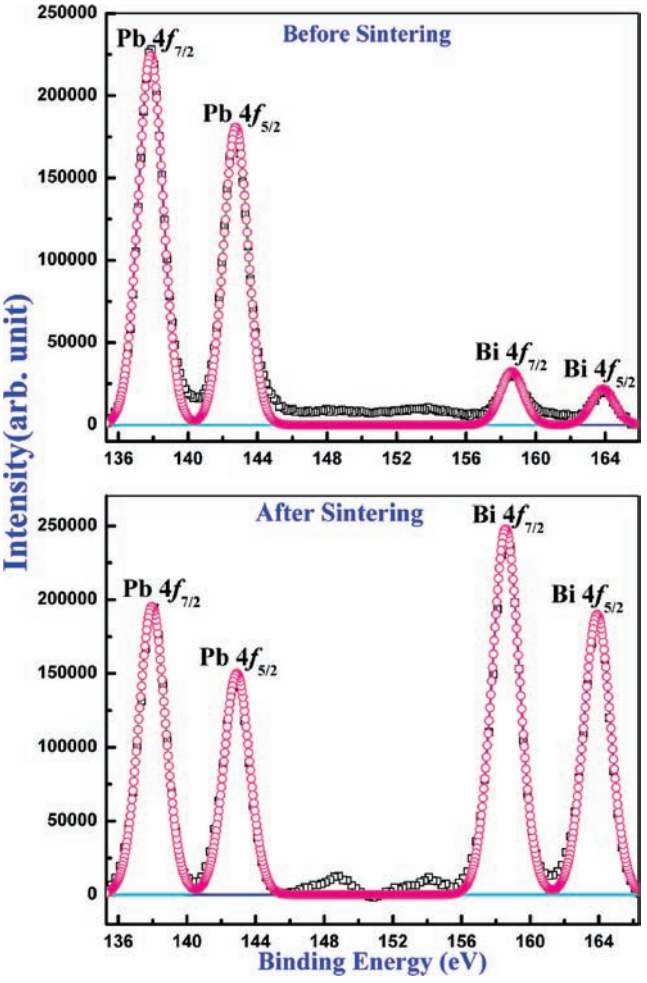

Figure 11. XPS spectrum of the sample $x = 0.50$ before and after sintering.

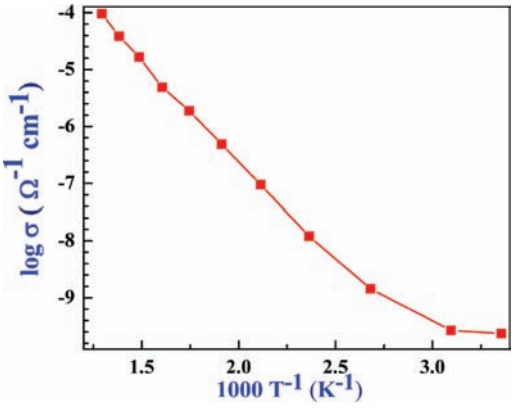

Figure 12. Ionic conductivity from ac impedance for $Pb_{2.5}Bi_{1/3}V_2O_8$.

palmierite $Ba_3V_2O_8$ and Nd^{3+}-doped $Ba_3V_2O_8$ were grown by the Czochralski technique for stimulated Raman scattering. The $Ba_3V_2O_8$ crystal was pale yellow in color, whereas the 0.76% Nd-doped crystal was purple in color.[24]

Ionic Conductivity. The value of the bulk ionic conductivity was calculated from the intercept of the single semicircular arcs obtained in the complex impedance plots of Z' vs Z''. $Pb_{2.5}Bi_{1/3}V_2O_8$ shows an order of 10^{-4} Ω^{-1} cm^{-1} at 500 °C. The conductivity measurements in the form of an Arrhenius plot ($\log \sigma$ vs $1000/T$) are shown in Figure 12.

The linear behavior of log σ with $1/T$ (Figure 12) indicates the absence of any phase transition, as shown from powder XRD data. The conduction mechanism cannot be due to anion migration. It could be either cationic or electronic or both. A solid solution, $Sr_{2.4}La_{0.4}(V_{1-y}P_yO_4)_2$, with the palmierite structural type shows conductivity, primarily because of the formation of vacancies and interstitial Sr ions with an increase in the temperature.[23] In the present study, because both Pb and Bi atoms are heavy to migrate, the conductivity mechanism may be attributed to the creation of vacancies, which would have appeared because of the substitution of Pb^{2+} by Bi^{3+}.

Conclusions. A new solid solution in the phase diagram of $Pb_3V_2O_8-BiVO_4$ has been isolated. The crystal structure of $Pb_{2.5}Bi_{1/3}V_2O_8$ has been determined by combined single-crystal XRD and NPD. The various compositions synthesized above and below the solid solution limit indicate that the range of the solid solution is narrow. The upper and lower limits of the solid solution has β-$Pb_3V_2O_8$ and eulytite $Pb_3BiV_3O_{12}$ as additional phases along with the palmierite phase. No phase transition was found for the various members of the solid solution. XPS data prove the presence of the ppm level of Bi_2O_3 when the samples were sintered at high temperature and, hence, explain the change in color at high temperature. The conductivity property can be attributed to the presence of vacancies in the system.

Acknowledgment. P.P.S. thanks the Indian Institute of Science for a senior research fellowship and LAFICS (IFLACS) for financial assistance. We acknowledge funding (Grant DST-0858) from DST-India. We thank DST-FIST (level II) for funding the Oxford diffraction X-ray facility. P. P.S. thanks DST-India and Sincrotrone Trieste for financial support during the synchrotron data collection at Trieste, Italy. We thank Professor M. S. Hegde and Dr. Aninda J. Bhattacharyya for providing XPS and conductivity facilities. Thanks are due to Dr. Polentarutti Maurizio and Dr. Bais Giorgio for scientific assistance during the synchrotron data collection. We acknowledge support of the National Institute of Standards and Technology, U.S. Department of Commerce, for providing the NPD data. We thank Dr. Mark Green for conducting the neutron experiments.

Supporting Information Available: CIF files for the single-crystal XRD and NPD, full pattern matching of the powder XRD pattern of $Pb_{3-x}Bi_{2/3x}V_2O_8$ for $x = 0.10$ (Figure S1), full pattern matching of the powder XRD pattern of $Pb_{3-x}Bi_{2/3x}V_2O_8$ for $x = 0.75$ (Figure S2), and SEM micrograph of a single crystal (Figure S3). This material is available free of charge via the Internet at http://pubs.acs.org.